Department of Physics and Astronomy
Heidelberg University

Bachelor Thesis in Physics
submitted by

Valentin Friedrich Hahn

born in Bad Kreuznach (Germany)

2023

Design and Commissioning of an Optically Transparent Cryogenic Valve for the ALPHATRAP Experiment

This Bachelor Thesis has been carried out by Valentin Hahn at the
Max Planck Institute for Nuclear Physics in Heidelberg
under the supervision of
Priv. Doz. Dr. Sven Sturm

Abstract

A new cryogenic vacuum valve was developed for the ALPHATRAP experiment representing a revision of the cryogenic valve that was presented in [1]. An upcoming measurement campaign of the g-factor experiment ALPHATRAP is intended to measure the ro-vibrational spectrum of the HD^+ molecular ion using infrared lasers. The previous valve had to be opened to allow laser light to pass through, when working with the lasers. To ensure that the vacuum required for spectroscopy is not lost by keeping the valve open, the valve is redesigned to include a window. The addition of the CaF_2 window in the center allows for laser cooling and laser spectroscopy under extreme-high vacuum conditions. Its vacuum sealing properties were demonstrated both through theoretical estimates of the gas flow and through two series of measurements both in room temperature as well as cryogenic temperatures.

Überblick

Ein neues kryogenes Vakuumventil wurde für das ALPHATRAP Experiment entwickelt. Das neue Design stellt dabei eine Überarbeitung des kryogenen Ventils, das in [1] vorgestellt wurde, dar. Eine anstehende Messkampagne des g-Faktor Experiments ALPHATRAP soll das Rotations-Schwingungsspektrum des HD^+ Molekül-Ions mithilfe von Infrarot Lasern untersuchen. Da das vorherige Ventil kein Laserlicht passieren lässt, musste das Ventil häufiger geöffnet werden um mit den Lasern zu arbeiten. Um sicherzustellen, dass das für die Spektroskopie erforderliche Vakuum durch das offene Ventil nicht verloren geht, wurde das Ventil um ein Fenster erweitert. Das neue Design kann dabei auf einige Teile des Vorgängers zurückgreifen, aber mit der Erweiterung um das CaF_2 Fenster in der Mitte erlaubt es nun Laserkühlung und Laserspektroskopie unter extreme-high vacuum Bedingungen. Die Funktion wurde sowohl über theoretische Abschätzungen des Gasflusses, sowie durch zwei Messreihen gezeigt.

Contents

1 Introduction

Recent measurements on the electron magnetic moment and therefore electron $g-2$ were brought to unprecedented precision of 0.13 ppt providing a stringent test of the standard model [2]. While the prediction of the standard model agrees with their measurement, a recent result of the muon $g-2$ experiment [3] showed a discrepancy between the theoretical prediction and their measurement of 4.2-σ encouraging further quantum electrodynamics (QED) tests. The discrepancies of muon $g-2$ are particulary interesting for muonic systems like muonic atoms where only a muon is bound to an atomic nucleus. Due to the higher mass, the muon sits closer to the atomic nucleus resulting in a much higher interaction between the two particles than in highly charged ions (HCI). Testing QED in composite particles [4, 5, 6], allows to test the QED interaction between charged particles with extremely high precision while probing different systems allows testing of all aspects of the underlying theory. Like muonic atoms, hydrogenlike ions which consist of a nucleus with one bound electron allow precise theoretical predictions due to their simple composition while also providing a very strong electromagnetic interaction between the nucleus and the bound lepton. The crucial advantage of hydrogenlike ions over muonic systems is that they provide very long lifetimes within very good vacua making them suitable for high precision experiments. The investigation of QED in the strong fields provided by HCI will give a deeper understanding of QED potentially being sensitive for new physics [7].

ALPHATRAP is a high precision experiment that was initially designed to test QED in strong fields by measuring the Landé g-factor of HCI [8]. Since recently ALPHATRAP plans to perform measurements on single molecular hydrogen ions as well. These allow vibrational and rotational levels to be studied and compared to theory as well. To produce ions in a large range of different charge states, we need several ion production facilities [9, 10, 11, 12]. To reach very high charge states like $^{208}Pb^{81+}$ these become larger and require higher power and cannot be built into the cryogenic setup anymore, like it is done in other similiar Penning trap experiments that use in-trap ion sources [13, 14]. Relying on external ion production requires a room temperature beamline connecting the ion sources and the cryogenic trap tower. In the current setup at ALPHATRAP, the room temperature beamline is evacuated to a pressure of roughly $5 \times 10^{-11}\,\mathrm{mbar}$. Assuming this pressure in the measurement trap, the lifetimes of any ion of interest would be only several minutes.

Because of the low temperature of the trap, which is cooled by liquid helium, we expect an extremely good vacuum in the trap stack. But due to the injection of ions from the external sources, which are connected via the room temperature beamline, a strong inflow of gas is introduced saturating the surfaces and causing the vacuum to degrade if the experiment is not thermally cycled. Due to the relatively slow speed of the injected ions, a degrader foil [15] cannot be used, therefore requiring a free-space connection to the different sections. This can be solved by putting a valve into the cryogenic section that effectively closes the trap chamber off to the pressure of the room temperature beamline. To be able to perform a high-precision measurement without reloading, an ion lifetime of at least a month is needed. This in turn sets an upper bound on the effective pressure in the

trap to below 10^{-16} mbar for the ions we want to use. In the ALPHATRAP setup a cryogenic valve was installed at the beginning of its operation [1]. Its design proved to be successful for shielding the cryogenic vacuum section when closed while giving access to loading new ions into the setup when open.
The mechanism of the valve has to withstand a strong magnetic field, while being at the same time at cryogenic temperatures. Currently, ALPHATRAP has a system of manually actuated gears in place that is focused on not bringing too much heat load and torque to the cryogenic system.
For the new measurement campaign for laser spectroscopy of the ro-vibrational spectrum of HD^+ ALPHATRAP is currently being set up. A first laser spectroscopy study of the fine structure in $^{40}Ar^{13+}$ has been performed at ALPHATRAP in [16]. However the HD^+ spectroscopy will require infrared laser light of up to 100 mW in the 4.2 K section, which has less than 100 mW of overall heat load put onto it without the laser [8]. Laser light of this intensity will therefore introduce a large heat load onto the trap, which in turn sets the gas particles free that were previously frozen out on the heated surfaces giving a higher pressure and lower standing time. Furthermore, we need to be able to control and adjust the laser within the setup to hit the ion position properly. Thus far, the valve had to be opened in order to align the laser. This in turn allows gas from the room temperature section to stream into the trap, worsening the vacuum within. The solution for this is a window installed into the valve, which transmits the laser light while blocking off residual gas from the room temperature side. This will also prove valuable for studying laser cooling within the trap, which was already done with $^9Be^+$ in [17].
The setup and testing of this new cryogenic valve will be the main focus of this thesis. In Section 2, first the necessary vacuum physics will be discussed. The later sections cover the technology that goes into the requirements of the valve as well as the design of the new cryogenic valve with a window to transmit laser light while the valve is in its closed position.

2 Vacuum physics

In this chapter an overview of the physics of vacuum theory is given. More in depth details can be found in Reference [18].

2.1 Definition of vacuum ranges

To further understand the challenges that come up when performing measurements on a single ion we have to take a look at vacuum theory.
In order to get a uniform understanding for different grades of vacua the International Organization for Standardization (ISO) defined several ranges [19] as seen in Table 1. The pressures we are handling at ALPHATRAP are in the 10^{-11} mbar range at the end of the room temperature beamline and below 10^{-16} mbar at the Penning trap stack. So the experiment essentially operates in the XHV

Definition	Pressure range [mbar]	mean free path λ_{N_2} [m]
low (rough) vacuum	$1100 - 1$	$9.2 \times 10^{-8} - 10^{-4}$
medium (fine) vacuum	$1 - 10^{-3}$	$10^{-4} - 10^{-1}$
high vacuum (HV)	$10^{-3} - 10^{-8}$	$10^{-1} - 10^{4}$
ultra-high vacuum (UHV)	$10^{-8} - 10^{-11}$	$10^{4} - 10^{7}$
extreme-high vacuum (XHV)	$< 10^{-11}$	$> 10^{7}$

Table 1: Pressure ranges as given in [19]. The mean free paths λ_{H_2} are given for the hydrogen molecule at $0\,^{\circ}\mathrm{C}$ according to Equation 3.

range, in addition to the insulation and pre-vacua that operate in the HV range.

2.2 Mean free path

In kinetic gas theory the mean free path is given as the average distance a particle travels until it collides with another particle. Within the HV range this distance ranges from several centimeters rising up to many kilometers within UHV and XHV as seen in Table 1. These long mean free path lengths are essential when we consider storing charged particles for up to months within a Penning trap since we do not want any disturbance of our particle during an experimental cycle. A good approximation for the behavior of many gases is the ideal gas law that relates the particle density $n = N/V$ with the Boltzmann constant k_B, the temperature T and the pressure p of the gas within the volume V:

$$p = \frac{N}{V} k_B T = n k_B T \tag{1}$$

With this the mean free path of a particle λ within a medium can be defined as

$$\lambda = \frac{1}{n \cdot \sigma} = \frac{k_B T}{p \cdot \sigma} \tag{2}$$

Where σ is the cross section for the collision between the gas particles. The hard spheres model assumes that the gas particles have no charge and have certain diameter d. When we have a gas consisting of only a single particle type the cross section for the collision of a pair becomes $\sigma = \pi(2r)^2 = \pi d^2$ [20].

If we just plug σ into Equation 2 we assume that just one particle is moving while all others are standing still. When considering moving particles we have to take the relative velocities into account. For two particles with normally distributed velocities, the relative velocity will just consist out of the standard deviations of their velocities $v_{rel} = \sqrt{v_0^2 + v_0^2} = \sqrt{2} v_0$. We can now again consider all particles to be standing still while the one of interest is moving at v_{rel}. This then enlarges our the covered cross sectional area by a factor $\sqrt{2}$:

$$\lambda = \frac{1}{\sqrt{2} \pi d^2 n} \tag{3}$$

For the hydrogen molecule the kinematic diameter is $d = 2.89\,\text{Å}$ [21]. This can be used to calculate the mean free path within hydrogen gas as shown in the third column of Table 1.

2.3 Types of gas flow

The mean free path determines the character of the gas flow within a vacuum system. The type of gas flow can be described by the ratio of the mean free path and the smallest distance of the chambers walls. Depending on the geometry of the vacuum chamber and quantities like the mean free path or the pressure inside, there are three types of flow which we can differentiate:

1. When the mean free path of the gas particles is very large compared to the cross dimensions of the vacuum chamber, particles will not collide with each other anymore. They therefore move independent from each other through the line with their thermal velocity. Thus, the dominant interaction is the collision with the chamber walls getting reflected on them over and over again. Taking the average over many particle trajectories we can get a macroscopic flow dynamic. This is the range of the **molecular flow** which is driven by the thermal motion of the gas particles.

2. At sufficiently high pressure the mean free path is smaller than the cross dimensions of the vacuum chamber. Then the particles will primarily collide with each other constantly exchanging energy and momentum. Since there can be so many gas particles even in smaller volumes the gas particles are considered continuous. Therefore it is called the **continuum flow** or **viscous flow**. It is the classical type of flow which we experience daily at ambient pressure. Its main driving force are local pressure differences.

3. At intermediate pressures between the molecular and viscous flow we find a transition area. In this **transitional flow** or **Knudsen flow** we find that the collisions with the wall happen to the same extend as collisions with other gas particles.

To differentiate between the types of flow the Knudsen number Kn is defined as a dimensionless quantity given as the ratio between the mean free path of the gas particles λ and a characteristic length d of the vacuum system, for example the diameter of a gas tube.

$$Kn := \frac{\lambda}{d} \tag{4}$$

We can now give a range of this new characteristic to the three vacuum ranges. We are within the continuum flow when $Kn < 0.01$. The transitional flow ranges from $Kn > 0.01$ to $Kn < 0.5$. For $Kn > 0.5$ we find ourselves in the molecular flow regime. These definitions are taken from [18] and vary from textbook to textbook. However this categorization still serves as a good guideline. In order to classify where different parts of the ALPHATRAP setup fit into these categories, three exemplary components of the setup are given in Table 2 with their typical dimensions. We can see

component	char. diameter [mm]	pressure [mbar]	Kn
Ion optics beamline	66	10^{-10}	1.56×10^{7}
Pulsed drift tube	16	10^{-11}	6.25×10^{8}
Precision Trap (4.2 K)	18	10^{-16}	8.67×10^{13}

Table 2: Knudsen numbers for different parts of the experiment.

that we always are significantly higher than $Kn > 0.5$. Therefore we can say that the experiment will always operate within the molecular flow regime.

2.4 Quantifying gas flow

To quantify the gas flow we can define the flow rate q_V as the amount of gas transported per time. The amount of gas flowing can be described in terms of volume, mass or particle number. We will start by defining the volume flow rate as

$$q_V = \frac{\Delta V}{\Delta t}, \qquad [q_V] = \frac{\mathrm{m}^3}{\mathrm{s}} \tag{5}$$

When discussing pumping vessels that are evacuated by a vacuum pump, we can define the volume flow rate at the inlet of the pump as the pumping speed S. It is therefore also given in units of $\frac{\mathrm{m}^3}{\mathrm{s}}$ as in Equation 5.
The flow rate through a component has to be considered at different positions throughout the volume of interest. When we look for example at a tube, then the volumetric flow rate will change along its length due to a drop in pressure along the tube. For this reason the q_{pV} throughput can be defined, which approximately stays constant throughout a component assuming no additional leaks throughout a component. The concept of throughput or pV-flow q_{pV} can be defined as a function of the change in volume over time $\dot{V}$ and the pressure p:

$$q_{pV} = \frac{\mathrm{d}V}{\mathrm{d}t} \cdot p \qquad [q_{pV}] = \mathrm{mbar}\frac{\mathrm{l}}{\mathrm{s}} \tag{6}$$

q_{pV} has a linear dependence on the pressure p which intuitively can be explained by a higher pressure resulting in more particles in the same volume that can be moved at the same time.
Using the ideal gas law and the throughput we can derive the particle flow q_N:

$$q_N = \frac{dN}{dt} = \frac{d}{dt}\frac{pV}{k_\mathrm{B}T} = \frac{p}{k_\mathrm{B}T}\frac{dV}{dt} = \frac{q_{pV}}{k_\mathrm{B}T} \tag{7}$$

2.5 Vacuum conductivity

When we consider different vacuum chamber geometries we would expect that the gas flow within a structure is limited. This limitation can be expressed in terms of the flow conductance and flow

resistance. The gas flow q is then analogous to the electrical current and the pressure acts as an electrical potential. In that sense the flow resistance R is comparable to the ohmic resistance. They are defined as

$$R := \frac{\text{pressure difference}}{\text{flux}} = \frac{\Delta p}{q} \tag{8}$$

$$C := \frac{1}{R} = \frac{q}{\Delta p} \tag{9}$$

The units of these quantities depend on which type of definition is used for q. With q_V we would get units of $[R] = \frac{\text{mbar}\cdot\text{s}}{\text{m}^3}$ and $[C] = \frac{\text{m}^3}{\text{mbar}\cdot\text{s}}$ and for the more often used q_{pV} we get $[R] = \frac{\text{s}}{\text{l}}$ and $[C] = \frac{\text{l}}{\text{s}}$.
Similar to electrodynamics we can define a total resistance R_{tot} and a total conductivity C_{tot} of a series or parallel connection of vacuum parts:

$$\text{Series connection:} \qquad R_{\text{tot}} = R_1 + R_2 + R_3 + ... \quad \text{and} \quad \frac{1}{C_{\text{tot}}} = \frac{1}{C_1} + \frac{1}{C_2} + \frac{1}{C_3} + ... \tag{10}$$

$$\text{Parallel connection:} \qquad C_{\text{tot}} = C_1 + C_2 + C_3 + ... \quad \text{and} \quad \frac{1}{R_{\text{tot}}} = \frac{1}{R_1} + \frac{1}{R_2} + \frac{1}{R_3} + ... \tag{11}$$

These equations are analogous to electronics, but do not always give the full picture. Equation 10 in theory holds only for components which are separated by larger volumes. This is because the inflow of a component will decrease if it has the same or a smaller cross section as the previous section. Since the inflow of the first part directly goes into the resistance of this second part, we would need to correct for that. Similarly, the equation for the parallel connection only holds if the components have enough distance between each others inlets so that their inflow is not affected by each other.
Typically, in vacuum systems the conductance of apertures and tubes is given. For both conductances Reference [18] gives empirical formulas to estimate their values. The conductance of molecular flow through an aperture can be calculated in terms of gas volume per second:

$$C_A = \frac{\bar{c}}{4} A = \frac{A}{4}\sqrt{\frac{8RT}{\pi M}} \qquad [C_A] = \frac{\text{m}^3}{\text{s}} \tag{12}$$

where $\bar{c}$ is the mean thermal velocity, A is the area of the aperture, R is the universal gas constant, T is the temperature and M is the molar mass. For a aperture with an area of $A = 1\,\text{cm}^2$ with air at $20\,^\circ\text{C}$ we get a conductance of $C_A = 11.6\,\frac{\text{l}}{\text{s}}$ from a thermal velocity of $463\,\frac{\text{m}}{\text{s}}$. The conductance of a long tube with a circular cross-sectional area is given in Equation 13. For this tube to be defined as long, the length l must be significantly larger than its diameter d.

$$C_{T,long} = C_A \cdot \frac{4}{3}\frac{d}{l} = \frac{d^3}{12l}\sqrt{\frac{8\pi RT}{M}} \qquad [C_T] = \frac{\text{m}^3}{\text{s}} \tag{13}$$

All the definitions of the parameters stay the same as in Equation 12 above.

2.6 Ion lifetimes

The discussion of the lifetime is based on the absorbing sphere model described in [22] and while its application to the Penning trap is based on [23].
At ALPHATRAP, the aim is to store ions as long as possible for the measurement campaigns. To be able to store an ion over an extended measurement campaign we need to have the best vacuum possible. Only then we can ensure that the charge state of our ion of interest does not change over the duration of our measurement. A measurement campaign lasts a few months and preferably, the same ion is used during this time to ensure the same environment and systematics which might change by reloading ions.
For HCI, the dominant loss process is electron capture. At 4.2 K the residual gas will mainly consist of helium atoms and hydrogen molecules. This is because these are the only gases that are not perfectly cryopumped by the surrounding walls, more details can be found in Section 3.3. For the analysis of the ion lifetimes it is sufficient to only consider helium atoms to simplify the discussion, as this will not cause a large error within this estimation of the lifetime [1, 23] and molecular effects can be neglected.
To analyse the probability of collision we can start with the mean free path of our stored ion within a helium background pressure of p. It is given by:

$$\lambda(\tau) = \hat{v}\tau \quad \text{with} \quad \hat{v} = \sqrt{\langle v_{\text{He}}^2 \rangle + \langle v_{\text{ion}}^2 \rangle} = \sqrt{3k_{\text{B}}T\left(\frac{1}{m_{\text{He}}} + \frac{1}{m_{\text{ion}}}\right) + (R_{\text{cyc}} \cdot \omega_c)^2} \tag{14}$$

Where $\hat{v}$ is the mean thermal velocity of the system and τ is the corresponding mean free time. Penning traps confine the ions within an energetic radial motion called the cyclotron motion [8]. Therefore, the average velocity of the ion is defined by its thermal energy $E_{\text{therm}} = \frac{3}{2}k_{\text{B}}T$ and its cyclotron excitation energy $E_{+,\text{exc}} = \frac{1}{2}m_{\text{ion}}(R_{\text{cyc}} \cdot \omega_c)^2$ describing its motion at the cylotron radius R_{cyc} with the eigenfrequency ω_c. ω_c is different for arbitrary ions, it scales with $\omega_c \propto \frac{q}{m_{\text{ion}}}$. But for HCI it can be estimated as $\omega_c \propto \frac{1}{2}\frac{e}{u}$. This translates to $\omega_c \approx 30\,\text{MHz}$ within the ALPHATRAP Setup. From the energy relation $E_{\text{therm}} = E_{+,\text{exc}}$, the cyclotron radius R_{cyc} is given as $R_{\text{cyc}} = \sqrt{\frac{3k_{\text{B}}T_{\text{cyc}}}{m_{\text{ion}}\omega_c^2}}$. Here the temperature of the cyclotron mode $T_{\text{cyc}} \neq T = 4.2\,\text{K}$. When the axial motion is coupled to the 4.2 K resonator, we will have $T_{\text{cyc}} = \frac{\omega_+}{\omega_z}T \approx 160\,\text{K}$ [8]. Putting both Equation 14 and 2 together we obtain

$$p = \frac{k_{\text{B}}T}{\sigma\hat{v}\tau} \tag{15}$$

When we know the cross section σ we can discuss the pressure needed for a given ion to achieve a certain storage time. Equivalently we can also describe τ as the average time until the ions capture an electron from a residual gas particle. A semi-empirical formula for the cross section for electron

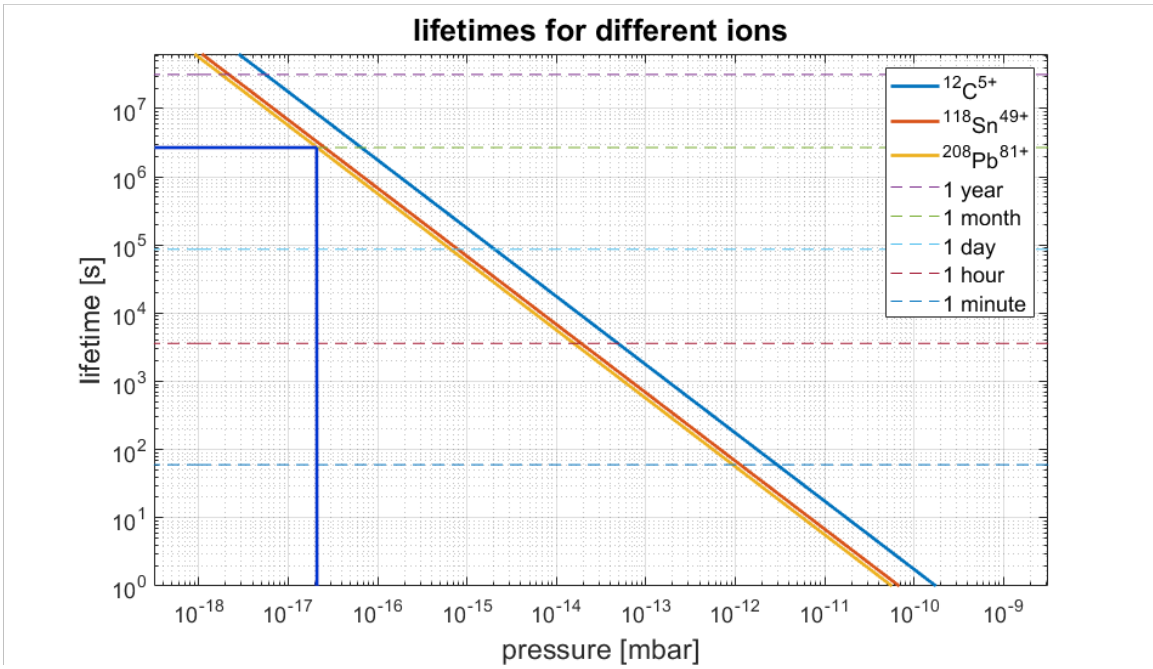

Figure 1: Lifetime as a function of pressure for $^{208}Pb^{81+}$, $^{118}Sn^{49+}$ and $^{12}C^{5+}$ with helium atoms as residual gas. Marked in the plot is the pressure corresponding to one month of lifetime within hydrogenlike lead.

transfer between ions with charge and neutral particles is given in Reference [22] in atomic units as

$$R_c^2 e^{-2.648\kappa R_c/\sqrt{q}} = 2.863 \cdot 10^{-4} q(q-1)\frac{\hat{v}}{f} \quad \text{and} \quad \sigma = \pi \cdot R_c^2 \tag{16}$$

Where we have $\kappa = \sqrt{\frac{I_p}{13.6\,\text{eV}}}$ with the ionization potential I_p of the neutral particle in eV, the charge of the ion q, the Franck-Condon factor f which only comes into play for molecular collisions ($f = 1$ otherwise) and the critical radius R_c as the distance at which internuclear interactions dominate. The ionization potential for single electron capture of a neutral helium atom is $I_p \approx 24.6\,\text{eV}$ [24]. With this we can then calculate R_c to find the cross section σ for a specific ion species. Figure 1 shows the ion lifetimes in the trap are plotted against the pressures from UHV into the deep XHV range. The figure shows the lifetimes of $^{208}Pb^{81+}$, $^{118}Sn^{49+}$ and $^{12}C^{5+}$ within helium residual gas. The latter two have already been used for different measurement campaigns [6, 25], whereas $^{208}Pb^{81+}$ would be part of a future measurement campaign with new ion production facilities [12].
We can clearly see that to be able to have lifetimes longer than a month we need a vacuum that is at least of the order of $6 \times 10^{-17}\,\text{mbar}$ for carbon or $2 \times 10^{-17}\,\text{mbar}$ for lead. This is a challenge in terms of vacuum technology for a Penning trap with external ion sources connected via a room temperature beamline.

3 ALPHATRAP setup and vacuum technology

3.1 Room temperature beamline

The ALPHATRAP setup is designed to be able to perform spectroscopy on HCI as high as lead $^{208}Pb^{81+}$. To get such highly charged ions into the trap we need sophisticated ion production facilities.
ALPHATRAP has access to three different ion sources [9, 10, 11], which are able to produce ions within different ionization energy ranges.
All of these ion sources are on the ground floor above the basement, where the experiment with its 4 T magnet is located. They are connected through a room temperature beamline to the Penning traps below. The ion sources beamline is permanently pumped via several turbomolecular pumps. While the vertical beamline towards the trap tower is additionally pumped with NEG and ion getter pumps, since when the valve is open we get a free path directly to the ion position that any residual gas particle could take. Additionally, the room temperature section is baked out when parts of the vacuum chamber were exchanged or had to be vented, in order to ensure a good vacuum. This way the vacuum chamber reaches a vacuum of down to 10^{-11} mbar. As discussed in Section 2.6 this room temperature pressure would not be sufficient to store ions for the duration of the current measurement cycle.

3.2 Cryogenic setup

ALPHATRAP uses a combination of three distinct Penning traps to determine the g-factor and is designed to be able to measure g-factors of ions up and beyond hydrogen-like lead. These Penning traps necessitate a strong static magnetic field to confine the ions radially which is produced by a superconducting 4 T magnet in which the traps are placed. Good vacuum is needed to ensure that the ion remains in the charge state of interest during the measurement cycle. Collisions with residual gas result in transfer of electrons and thus in lowering the charge state of a highly charge ion. While the magnet has to be cooled to 4.2 K in order to remain superconducting, cooling the trap tower itself to the same temperature comes with the benefits of reducing noise, lowering systematic effects and enabling cryopumping, which dramatically improves the vacuum at the ions position, see Section 3.3. Vacuum chambers attached to the top of the trap chamber connect it to the ion sources, located at room temperature in the floor above the experimental setup. A section through the 3D-model of this setup is shown in Figure 2. The ions are injected from the upper floor in vertical direction into the setup. They pass the cryostat with its liquid nitrogen and helium tanks through a 0.9 m steel tube to reach the trap chamber. At the top of this tube the cryogenic vacuum valve is located. In the picture, we can see that the actual Penning traps are only in the bottom third of the 1.40 m long 4.2 K section, which is marked pink in Figure 2. The 4.2 K section is protected from room temperature heat radiation by the 77 K section, which is marked in blue, as well as the insulating

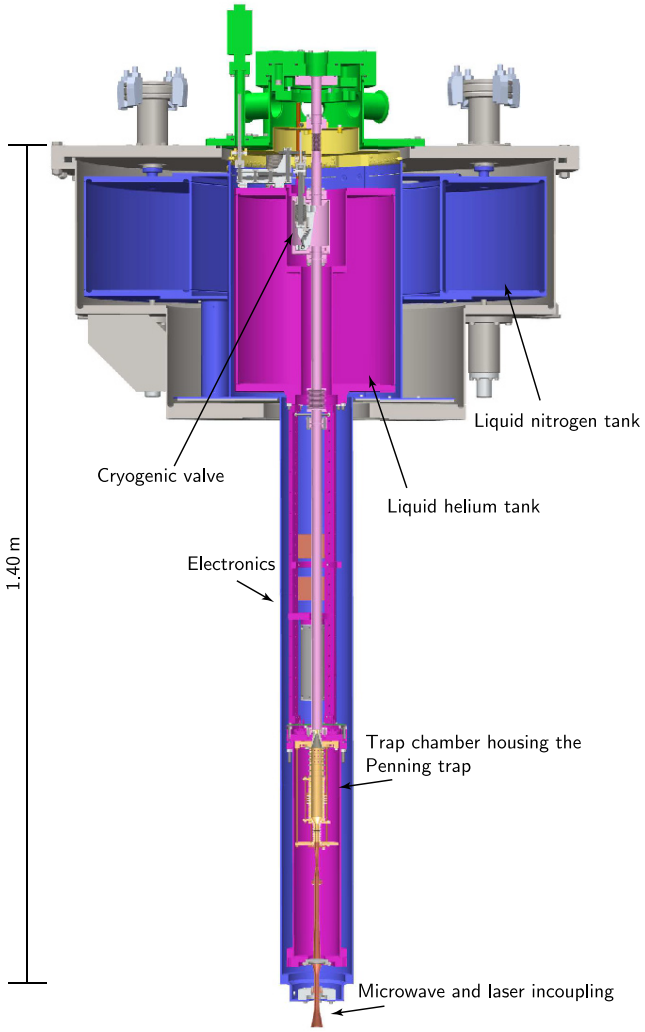

Figure 2: Picture showing the cryostat setup of ALPHATRAP. The blue and pink parts symbolize parts that are cooled down to 70 K by liquid nitrogen and 4.2 K by liquid helium respectively. The tube below the cryostat tanks are located within the superconducting magnet. In the bottom part the Penning trap tower as well as the Microwave incoupling are shown. Picture taken from [8]

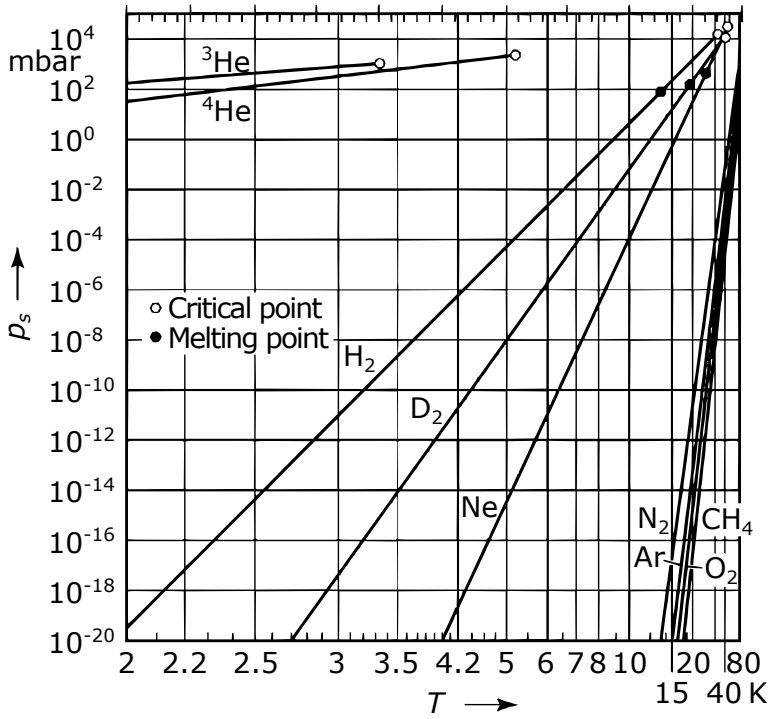

Figure 3: Saturation vapor pressures p_s of selected gases in cryogenic temperatures between $T = 2\,\mathrm{K} - 80\,\mathrm{K}$. Picture taken from [18].

vacua of the cryostat and the magnet. The magnet is positioned directly below the cryostat and is not shown on the picture.

3.3 Cryopumping

This section is based upon information found in Reference [18]. Cooling the experiment down will not only give us less thermal noise for the high-precision measurements, but will also lower the pressure within our trap chamber through cryopumping. This makes use of the long steel tubes that lead to the trap chamber which provides the surface area necessary to apply this technique. In a cryogenic vacuum pump the residual gases condense or adsorb onto cold surfaces. Ideally, the saturation pressure of the gases is lower than the pressure in the vacuum chamber. As we see from Figure 3, at $4.2\,\mathrm{K}$ the saturation vapor pressures of almost all residual gases are already in the range of below $10^{-18}\,\mathrm{mbar}$. So most gases will convert from their gaseous form to their liquid or even solid form and therefore do not contribute to the vacuum pressure in the chamber. Above $10^{-16}\,\mathrm{mbar}$ the notable exceptions at $4.2\,\mathrm{K}$ are ^{3}He, ^{4}He, H_2 as well as D_2, these are all still above

their saturation vapor pressure. To further get rid of these gases a more complex mechanism of cryosorption plays a role. The gas particles are bound to the cold surface with complex physical adsorption forces. These are not only temperature dependent, but also rely on the type of surface that is used. Therefore nanoporous materials with a high surface area like for example charcoal are frequently used to achieve a high cryosorption. The adsorption phase equilibria for a given temperatue will always sit below the saturation vapor pressures, giving access to a way of pumping even hydrogen or helium gas particles [26].
Through both mechanisms the gas particles will stay on the surfaces. Cryopumping is therefore limited by the space that is available on the surface of the cryopump as well as the pressure inside the chamber. To estimate the space inside of the chamber we can define that if all monolayers on the pumps surface are filled the pumping is saturated and the surfaces have to be cleaned. While this does not represent the real world condition where multiple layers can be filled up, this will serve as a conservative estimate. At ALPHATRAP, the consequence of this saturation is that the whole trap tower needs to be warmed up until all the gas evaporates from the surfaces while the chamber is pumped back down with a conventional vacuum pump. This also makes cryopumps difficult to use at higher pressures since the walls will get saturated regularly. A time scale for this saturation will be given in Section 3.4.3.

3.4 Vacuum flow within the cryogenic section

Right above the cryostat the vertical beamline enters the cryostat and therefore also the $4.2\,\mathrm{K}$ section. The pressure at this stage is roughly at $10^{-11}\,\mathrm{mbar}$. From this point the trap chamber with the Penning trap is located roughly $90\,\mathrm{cm}$ below being connected over steel tubing with a diameter of $16\,\mathrm{mm}$. In the inlet of the trap chamber sits the ion injection diaphragm as well as a microwave damping cone. These components reduce the inlet diameter to the trap chamber to just $3\,\mathrm{mm}$.
To estimate the pressure at the ions position we have different options. If we first assume that the long tube will freeze out every particle that hits it, then pressure at the ion would only be defined by the particles that travel all the way from the room temperature section towards this far away hole in a direct line. Collisions with residual gas particles are neglected, since at $10^{-11}\,\mathrm{mbar}$ we are already at $\lambda > 10^7\,\mathrm{m}$ (see Table 1) so within the molecular flow range.
Another way to look at it is that we do not freeze out every residual gas particle and have a molecular flow through the tube into the trap chamber through an aperture of $3\,\mathrm{mm}$ diameter. We can assume that we are within the first model, when the tube is fully cleaned of any gases that might already be stuck to it. When the system then becomes saturated, due to adsorption and desorption the second model better fits the system, where the molecular flow is described while taking diffuse reflections from the walls into account. Both descriptions are approximations, but should be able to show what kind of vacuum we can expect within the trap to begin with.

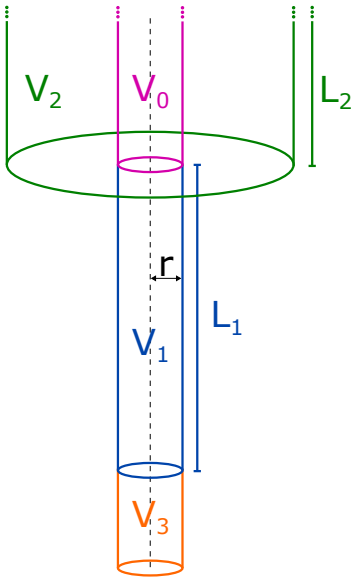

Figure 4: Visualisation of the model used for calculating the pressure inside the trap with an unsaturated ion tube

3.4.1 Unsaturated regime

For the unsaturated regime we can describe the pressure of the particle flow that reaches the trap chamber from the 1×10^{-11} mbar room temperature section by the following. The quantities and geometries described here are shown in Figure 4, while this discussion is based on [27]. To simplify, we can assume that there is a large volume V_2 sitting at this pressure. Below V_2 then sits the tube of length $L_1 = 90\,\text{cm}$ that connects the trap chamber volume V_3 to the beamline V_2. Since we assume, that every particle is absorbed at the wall of the tube, we only have to care for the particles inside a cylinder of radius $r = 1.5\,\text{mm}$ above the inlet to the trap chamber. We further assume that there is perfect vacuum below the beamline. When we consider a particle flow in the direction of V_3, we look only at the part of V_2, which sits right above the inlet to the trap chamber. The volume of this part is given as V_0. To simplify further, we want to assume that the cylinders of V_0 and V_2 are of infinite height L_2. We also will not pay attention to particles that come towards the inlet from an angle. Since this angle has to be very small for the particle to enter the trap chamber the influence of these particles will be negligible. This also includes the difference in radius due to the tube having a diameter of $16\,\text{mm}$, which we also do not consider here. At the beginning V_0 is filled with residual gas at $p_0 = 1 \times 10^{-11}$ mbar at room temperature. Due to the geometry discussed above the particles outside of V_0 can be neglected when only looking at the conductivity. First we want to calculate how many atoms within the volume V_0 are heading towards the inlet of the trap chamber, when we release all atoms of V_0 at the same time. The number of atoms inside V_0 is given as $N_0 = n_0 \cdot V_0$ with the particle density n_0 that can be calculated from the ideal gas law. For

the number of atoms N_1 that exit the cylinder V_0 towards V_1 we get

$$N_1 = \pi r^2 n_0 \int_0^\infty \frac{\pi r^2}{4\pi(L_1 + L_2)^2} \mathrm{d}L_2 = \frac{\pi r^4 n_0}{4L_1} \tag{17}$$

Where we integrated over the different relative solid angles of particles within V_0 in relation to the opening surface at the trap chamber. After this particle flow, V_0 will be empty with no particles inside anymore. From V_2 we now get a inflow of new gas particles due to the pressure p_0 that still prevails around V_0. The refilling will take place within a time frame of $\tau = \frac{r}{\bar{c}}$, where $\bar{c}$ is the mean thermal velocity of the residual gas. With this we can now give a particle flux I that leaves the tube V_1 towards the trap chamber V_3. It is given as

$$I = \frac{N_1}{\tau} = \frac{\pi r^3 n_0 \bar{c}}{4L_1} \tag{18}$$

This flow will then fill the cylinder V_3 below V_1. Within the time τ these atoms will hold a volume of $V_3 = \pi r^2 \bar{c} \tau$. With this we can now calculate the particle density n_3 within V_3 as the influx within the time τ:

$$n_3 = \frac{I\tau}{V_3} = \frac{I}{\pi r^2 \bar{c}} = \frac{n_0 r}{4L_1} \tag{19}$$

With $T_{\text{room}} \approx 293\,\text{K}$ and $p_0 = 1 \times 10^{-11}\,\text{mbar}$, we get $n_0 = \frac{p_0}{k_\text{B} T_{\text{room}}} = 2.47 \times 10^{11}\,\text{m}^{-3}$. From this we can calculate the pressure within the trap chamber as shown in Equation 20.

$$n_3 = \frac{p_3}{k_\text{B} T_{tc}} \quad \Rightarrow \quad \frac{n_3 \cdot T_{tc}}{p_3} = \frac{n_0 \cdot T_{\text{room}}}{p_0} \quad \Leftrightarrow \quad p_3 = p_0 \frac{n_3}{n_0} \frac{T_{tc}}{T_{\text{room}}} = p_0 \frac{r}{4L_1} \frac{T_{tc}}{T_{\text{room}}} \tag{20}$$

When we assume the gas that is now incoming into the trap chamber has a temperature of $T_{tc} = 4.2\,\text{K}$ we get $p_3 = 6.0 \times 10^{-17}\,\text{mbar}$ and for $T_{tc} = T_{\text{room}}$ we get $p_3 = 4.2 \times 10^{-15}\,\text{mbar}$. For the particle inflow from the room temperature beamline it should now be assumed that $T_{tc} = T_{\text{room}}$, since the particles went through the setup without collisions. From Figure 1 we could now get a lifetime of roughly a day for the lighter ions with $p_3 = 4.17 \times 10^{-15}\,\text{mbar}$.

3.4.2 Simulation within COMSOL

A simulation within COMSOL was performed in order to see the effect of full saturation of the tube. The physics engine used here was the trajectory of charged particles. To perform studies of residual gas the "charged" particles had $q = 0$ and a mass of $m = 2 \cdot m_{proton}$, representing hydrogen molecules. The simulation was set up around an axial symmetry on a 2D plane. The relevant part of the geometry is shown in Figure 5. An inlet at the top of the geometry was set to input particles according to a pressure of $1 \times 10^{-11}\,\text{mbar}$. This was done using the ideal gas law and Equation 12

for the conductance of an aperture C_A of a CF16 flange:

$$\dot{n} = n \cdot C_A = \frac{p}{k_B T} \cdot \frac{\bar{c}\pi r_{CF16}^2}{4} \tag{21}$$

The independent trajectories of each particle can then be calculated by the software. The trap chamber was modelled as a $30\,\mathrm{cm}$ high cylinder with a radius of $3.8\,\mathrm{cm}$. Above the trap chamber the conical shape of the insert was set with the internal radius at the thinner side of $1.5\,\mathrm{mm}$. Above that the $90\,\mathrm{cm}$ tube is located as before. To find the pressure at an ions position, the dimensions of the Capture Trap (CT) are used to define a volume where we can estimate the pressure. The CT is one of the three Penning traps used in the ALPHATRAP trap tower. It is used to store ions during a measurement and sits at the first position after the ions enter the trap chamber. It has a radius of $r = 9\,\mathrm{mm}$ and a height of $h = 46\,\mathrm{mm}$. To define the outcome of a collision with surfaces, the trap chamber walls were set to freeze out colliding gas, while all other walls were set to thermal reemission at $4.2\,\mathrm{K}$ and with the freeze out probability set to 0. To see the individual trajectories the time frame was chosen to be at $\Delta t = 1 \times 10^{-5}\,\mathrm{s}$, while the whole simulation took 100 cycles to map every particle. The particle density was calculated within the CT. For the first 30 iterations the equilibrium point was not reached yet. Therefore, the values for particle density here were not taken into account for the final steady state value.
With this steady state particle density the pressure can be calculated via the ideal gas law by the particle density within the CT. An room temperature equivalent pressure of $p = 2.12(13)\,10^{-16}\mathrm{mbar}$ was found, while the $4.2\,\mathrm{K}$ equivalent pressure was $p = 3.03(19)\,10^{-18}\mathrm{mbar}$. Where the error was given through taking the average. In Figure 5 we can clearly see that the main contribution to the particle density within the volume is given by the particles that traverse the inlet without any scattering at an angle. Therefore, the simulation verifies the assumptions made in the analytical estimation of the pressure. The difference in pressure resulting from the two methods is probably due to the different reference frame for which the pressure was calculated. The CT has a larger volume and radial expansion than V_3 which was used before. The simulation was done with the assumption that the tube is saturated, reemitting particles back to the chamber after a certain time. That the result is so close to the calculation done before shows that almost now particles cross the $0.9\,\mathrm{m}$ tube towards the trap chamber. The diffuse reflections will lead the particles out of the tube as well making this situation seem similar to the one calculated before. Taking this into consideration, the simulation validates the result obtained from the calculations showing that the pressure we can obtain without a valve is on the order of roughly $1 \times 10^{-15}\,\mathrm{mbar}$ which brings the ion lifetime to just above a day (see Figure 1).

3.4.3 Transition time

To know how long we will take to transition to a saturated tube, we can calculate the density of the particles on the surface of the steel tube. This density of a monolayer is given in [18] as

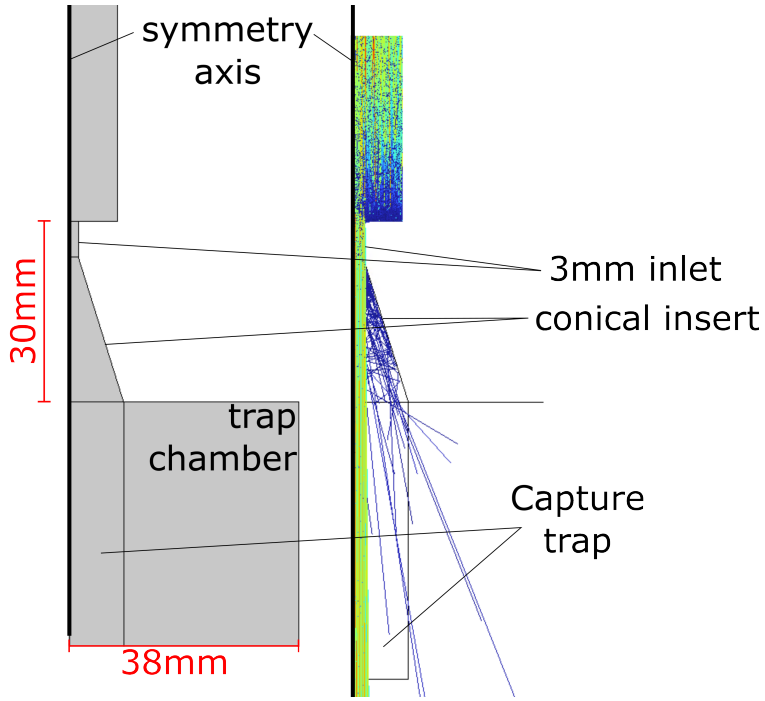

Figure 5: Geometry of the COMSOL Simulation. On the left is the plain geometry that was introduced with the conical inlet as well as the tube, the trap chamber and the inner volume of the Capture trap. The right side shows the simulation of the particle trajectories where the "colder" colors represent slower particles.

$n_{mono} = 1.13 \times 10^{19}\,\mathrm{m}^{-2}$. We can now calculate the inlet conductivity of a CF16 Flange at room temperature and $1 \times 10^{-11}\,\mathrm{mbar}$ in the molecular flow regime. This will give us the particle flow rate $\dot{n}$ from which we can calculate the time τ it takes the tubes cylindrical surface A_{tube} to be covered in one monolayer as shown in Equation 22.

$$\dot{n} = \frac{C_{CF16} \cdot p}{k_B T_{\mathrm{room}}} \quad \text{and} \quad \tau = \frac{n_{mono} \cdot A_{tube}}{\dot{n}} \tag{22}$$

This estimate is based on the assumption that all particles just linearly fill up the free spots on the steel tube without any prioritization of spots that come earlier within the tube. For an incoming particle flow of hydrogen at $M_{mol} = 2\,\mathrm{g/mol}$ we calculate a time of $\tau = 92\,\mathrm{hours} \approx 4\,\mathrm{days}$. This is not sufficient for a measurement cycle over one month.
From Equation 22 we can see that τ scales anti-proportional to the conductance so that when we lower the conductance we can improve the time that we have available before a monolayer of gas particles is frozen out on the ion tube. To do so we installed a cryogenic valve that is able to significantly lower the conductance of the CF16 flange within the $4.2\,\mathrm{K}$ section. This also reduces the main particle stream that is rushing towards the trap, since both methods used here show that the most particles that reach the ions position directly come down from room temperature vacuum towards the trap chamber. The valve limits this significantly, since all particles that directly move towards the trap chamber are now blocked on their immediate path. Additionally, the gas particles now thermalize on the tube section below, since they have to scatter to overcome the barrier that the valve represents. The current cryogenic valve that was introduced almost $9\,\mathrm{years}$ ago allowed long storage times of ions, for example 42 days for a Sn^{49+} ion after being thermally cycled before the measurement run. A more detailed look into how the valve works and what changes were made in the context of this thesis is explained in the upcoming sections.

4 Mechanical design of the cryogenic Valve

4.1 Design challenges

When it comes to designing the valve we first have to think about the requirements that the valve needs to fulfil. Commercially available vacuum valves have different problems, when it comes to this special use case here. First of all most common valves use sealing materials that eventually become porous at very low temperature. This already rules out a large number of valve types. Then we have to operate the valve within a strong superconductive magnet. This means that the material used must be non-magnetic to a high degree. The strong magnetic field rules out conventional electric motors as they will not work within the strong field. To ensure a proper torque the valve is therefore operated by hand. The vacuum range we are working in also sets boundaries on the valves, since most vacuum technology is not designed to be operated in XHV. While the outside

of the valve will be operated at HV to ensure no leakage into the ion tube. Vacuum greases that ensure reliable mechanical movement cannot be used here since their lubrication mostly freezes out at 4.2 K temperatures. Our setup is very sensitive to small displacements, hence we want to bring very little forces into our system to keep the position as it is. This will benefit the three polyimide rods that carry the weight of the inner 4.2 K section, since they should not become bend or lengthened by the operation of the valve. Additionally the material of these rods is chosen to have minimal heat conductivity increasing the standing time of the experiment. A valve that is operated from the room temperature section must therefore also ensure that this connection does not introduce a major heat load onto the liquid helium tank.
With the new design iteration of the valve we introduce a laser window into the setup. The window should be able to transmit wavelength from 313 nm for $^9Be^+$ laser cooling up to 5 µm for new spectroscopy and laser cooling campaigns. Additionally, it will enable us to align the laser along the traps axis without opening the valve, as shown in the previous section worsens the vacuum. Additionally, to drive weak transitions, often high laser power is required, in particular in the upcoming run a relatively high power of 100 mW is needed. The new design makes sure, that this laser will not heat up any parts of the 4.2 K section.
However, the main task of the valve is that it should lower the conductance through the valve significantly so that the trap chamber sits below 10^{-16} mbar for many months. In Section 3.4.1 it was shown that without a valve the trap chamber would sit at a pressure of $p_{tc} = 4.17 \times 10^{-15}$ mbar. This pressure can be reduced by limiting the incoming particle flow, since that will directly lower the particle density we get inside the trap tower. In Equation 21 we can see that lowering the conductance will in turn directly lower the incoming particle flow, which can be used to achieve a pressure that is below $p_{tc} = 1 \times 10^{-15}$ mbar. As seen in Section 3.4.1, the particles reaching the trap will most likely still be at room temperature. If we now block the main particle stream as well, we can make sure that every particle has thermalized at the walls due to the diffuse reflections needed to traverse the valve. We can also see from Equation 22 that the time needed to saturate the tube τ also scales with $\propto 1/d_{\text{tube}}^2$ and with only a CF16 flange as an inlet we obtain a time of 4 days. Lowering the conductivity again by two orders of magnitude will bring us up to 400 days, which is more than enough for our purposes.

4.2 Previous design

The first valve design that was used at ALPHATRAP over the last years worked very well fulfilling all these requirements. It was first setup 2014 during the master thesis of M. Oreskovic [1] and since then no modifications were made to the valve.
This design is shown in Figure 8 a). The valve gets actuated with a rotating rod in the room temperature section, shown in Figure 6. Actuation is done manually since the valve does not have to be opened often and this gives good controllability over the force that is put onto the mechanism. The rotation is then carried over towards a gearbox, see Figure 7, which sits above the 4.2 K stage

of the cryostat, also shown in Figure 6. The gearbox ensures that the torque which is applied to the valve itself stays low minimizing the stress to other components the valve is connected to. We also do not want to move the trap setup when we open and close the valve. The gearbox is then connected to a threaded rod that translates the rotation into a vertical movement of a brass carriage the threaded rod is connected to, see Figure 8 c). To now translate to the inner vacuum of the experimental setup the carriage pushes onto another rod that is mounted inside an edge-welded membrane bellow. The bellow separates the insulation vacuum from the XHV in the inside of the valve while still allowing movement of the part, even at cryogenic temperatures. Inside the valves housing the bellow is connected to the valves mechanical parts to finally close the valve turning the vertical motion of the bellow back into a leverage towards the seal. The outer enclosure and the outer mechanism are shown in Figure 8 c). The cylindrical enclosure itself is rather small with a diameter of $63.5\,\mathrm{mm}$ and a height of $90\,\mathrm{mm}$.

The sealing of the valve was then controlled via a steel disc that closed onto a CF16 sized copper flange. The disc was designed to have some play when pressed down to ensure that small misalignments are compensated. The play introduced was just for angular movement of the disc. No planar movement of the center of the disc relative to the seat was possible therefore aligning both central axes of the disc and the seat. This was done with a ball shaped head of the disc sitting within a conical holder piece both positioned central above the ion tube.

4.3 New design

The main goal was to make laser transmission out of the cryo section possible without degrading the cryo vacuum. This made an upgrade to the valve necessary. Since the first valve proved to be very reliable the idea of the previous design was expanded while some parts could be reused in the new design.

Most importantly, the alignment feature had to be redesigned since a laser window needed to be introduced directly central within the ion tube. The mechanism is shown in Figure 9. In the course of the thesis, advantages or disadvantages of different methods were discussed, and ultimately a spring loaded misalignment correction was chosen that still keeps the central part of the ion tube clear for the laser path. In the new design a rectangular steel plate, with the glass mounted directly on top, is mounted with 4 springs on each of the corners of the guiding piece. This way, the lever will first compress the springs, which compensates for a possible misalignment. The new mechanism will therefore still provide angular alignment additionally making use of the translational adjustment the springs can provide. In order to get springs of the right dimensions, a copper beryllium wire with a thickness of $0.6\,\mathrm{mm}$ was wound around a $3\,\mathrm{mm}$ rod, resulting in springs with an outer diameter of roughly $4.6\,\mathrm{mm}$. Their unloaded height was measured to be $3.50(5)\,\mathrm{mm}$ at 2.5 windings. Inside the holder they get preloaded to a heigt of $3\,\mathrm{mm}$.

For the transparent component an uncoated calcium fluoride $2\,\mathrm{mm}$ thick, flat window was chosen since it has a very broad range of high transmission starting below $300\,\mathrm{nm}$ and going beyond $5\,\mu\mathrm{m}$

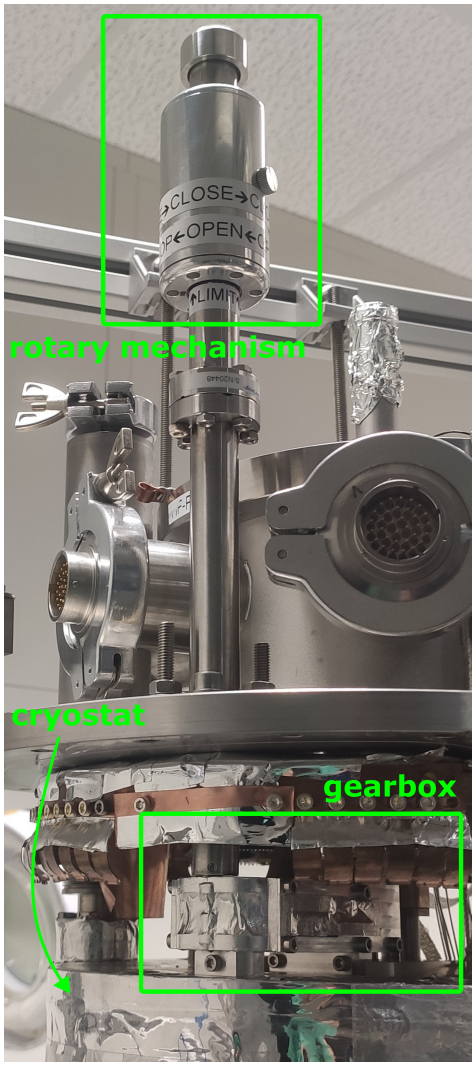

Figure 6: Picture of the Setup with the room temperature top flange with the actuation mechanism. Below the flange sits the gearbox, which is mounted to the cryostats liquid helium tank.

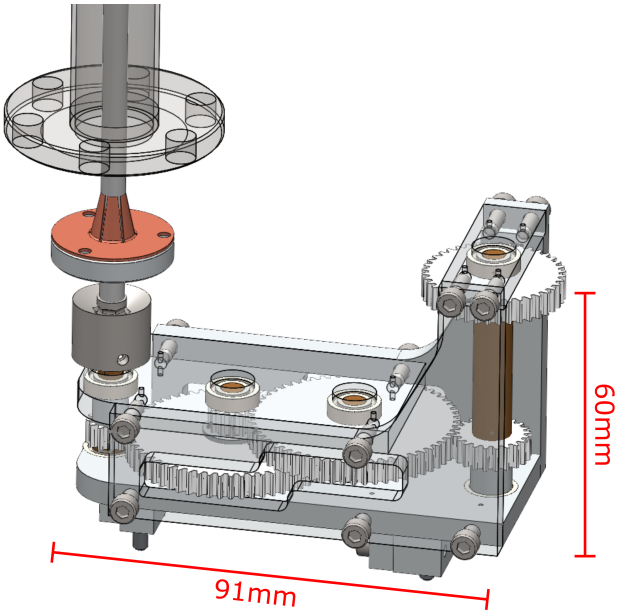

Figure 7: Model of the gearbox with a transparent side wall. The gear at the right is connected to the gear seen in Figure 8 c), when the valve is inside the setup.

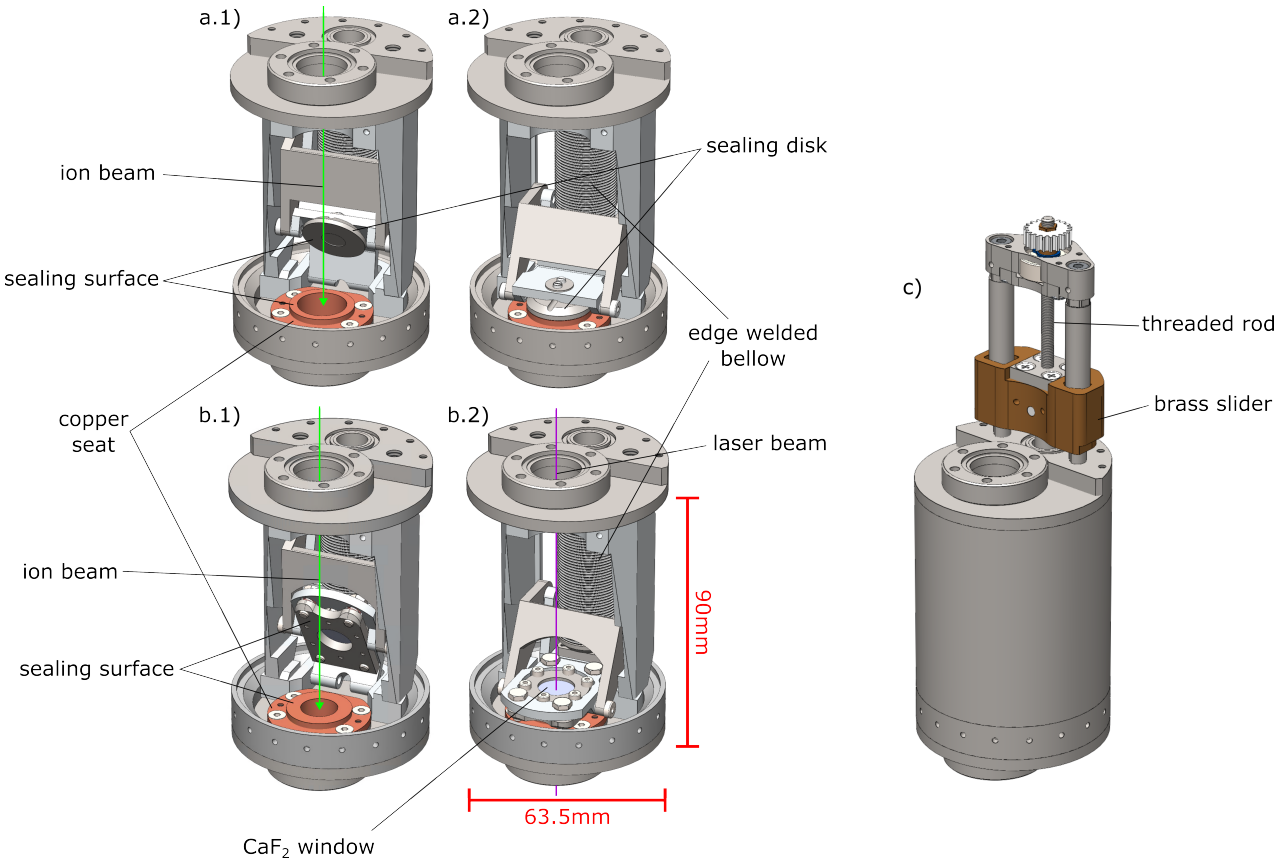

Figure 8: Shown are the two iterations of the valve. (a) previous design from [1]. (b) new design with the changes discussed in Section 4.3. (1) shows the valves in its open position, (2) in the closed. (c) The valve from the outside

which set the boundaries for potentially used laser wavelength within the upcoming spectroscopy measurements at ALPHATRAP. The advantage of using calcium fluoride over more conventional materials like sapphire or fused silica is its broad transmission range which will give the most flexibility for future projects. To seal the window onto the closing lid of the valve $200\,\mu m$ thick indium foil was used below and above the glas. A steel bracket mounted by six screws is firmly pressing the indium foil above and below the window, sealing the glass on top of the moving lid and compressing the foil down to $150\,\mu m$. The steel bracket has a hole with a diameter of $12\,mm$ while the window has a diameter of $15\,mm$.
Compared to the steel bracket the glass will not shrink significantly, while steel will reduce in size by $0.3\,\%$ [28]. The steel holder therefore has to have a recess of at least $1.003 \cdot 15\,mm = 15.05\,mm$. In the final model the steel bracket has a diameter of $15.4\,mm$, which will even account for indium being spread into that space. To test this the sealing piece was evacuated inside a tube that was then cooled down within liquid nitrogen. This was done to test whether the bracket would destroy the glass during a cool down in the experiment. After a successful test, the piece got mounted into the valve.

5 Estimation of the valves conductance

To quantify how this type of cryogenic valve performs we want to give a theoretical estimate of its performance that later can be compared to measurements performed on the constructed valve.

5.1 Slot model

A simple approach to calculating the conductivity of the valve is to model the valve as a rectangular slot. In this way we say that the two sealing surfaces have a constant distance between each other that is on the order of their surface roughness. The sealing surface is shown in Figure 9. The calculation is then similar to Equation 12 with a modification in terms of the transmission probability for a narrow slot as given in [18]:

$$C = P \cdot \frac{\bar{c}}{4} \cdot A \quad \text{with} \quad P = \frac{1 + \ln(0.433\frac{l}{b} + 1)}{\frac{l}{b} + 1} \tag{23}$$

Where l is the length of the slot, b is the height and a is the width. For the narrow slot here we must have $b << a$ which is the case for our model here. As a good estimation for the length of the slot is the distance between the thread of the glass holder and the $d = 12\,mm$ inner diameter hole. This length is $l = 3.2\,mm$, it can be found in Figure 9. When the upper sealing piece is misaligned this will deviate a bit, although the sealing surface extends past this length giving a better seal than assumed in this estimation. For the width of the slot we can take the mean circumference of the sealing surface at a diameter of $a = d + l = 15.2\,mm$.

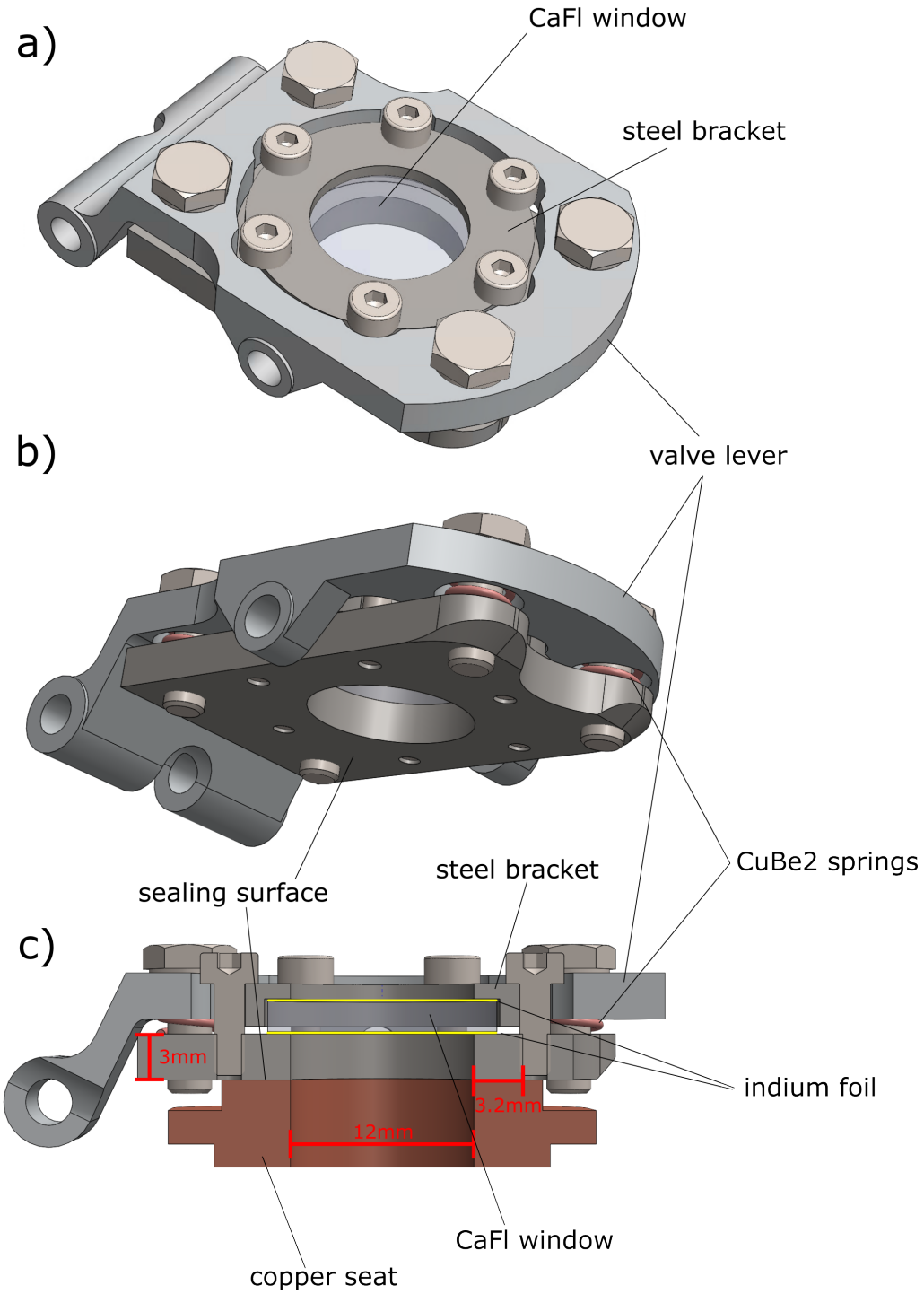

Figure 9: (a) The sealing flap from the top. The steel bracket as well as the mounting screws can be seen here. (b) Bottom view of the sealing surface. (c) Cut of the sealing flap inside the valve with the glass seal on top.

For a slot of $b = 10\,\mu\text{m}$ which should serve as a reasonable estimation of the surface roughness and helium as a residual gas at $4.2\,\text{K}$ we would get a conductivity of $C_{\text{closed}} = 0.000\,33\,\frac{\text{l}}{\text{s}}$. Comparing this to the open valve which then approximately consists of an aperture with a diameter of $d = 12\,\text{mm}$, we get $C_{\text{open}} = 4.2157\,\frac{\text{l}}{\text{s}}$. This gives a reduction in sealing of $C_{\text{open}}/C_{\text{closed}} \approx 12800$ which is much more than what we require. This factor will of course drop rather fast with the sealing height b. At $b = 20\,\mu\text{m}$ we only are at a factor of 3600 which still is enough.

5.2 Vacuum gasket model

The conductance through a more complex description of the geometry of a sealing surface is given in [29]. The authors discuss how a gasket and a vacuum flange seal off the vacuum during different stages of the sealing process. To do so they defined two different stages of the sealing that are positioned along their force cycle while tightening or releasing the flange. A visualization of these is given in Figure 10. The model assumes that the surface roughness is given by this periodical triangular surface with a fixed widths and angles α and β. The first stage of sealing is given by the two surfaces just touching each other. Here deformation will only take place in the softer material. The gaps that are left between the seals are given by their respective surface roughnesses and they will open gas channels that have a conductance C_0. The conductivity of these channels is given by the waviness parameters a_{m0} and A as defined in Figure 10 1). This stage is called accomodation stage. With rising pressure put on the seal the gasket will deform until a_m reaches 0 at which point the normal sealing stage starts, see Figure 10 2). At this stage the softer gasket material is pressed into the surface of the harder flange material, see Figure 10 3). Since the compression is mostly inelastic, the gasket will stay deformed after releasing. This will shrink A to a smaller A_r, while the two surfaces unite. When we further compress the gasket, we will be able to lower the conductance. To know in which stage of sealing we are in, we have to estimate the pressure we can put on the sealing surface. To estimate the force we put onto the sealing surfaces, the force required to compress a copper spring by $1\,\text{mm}$ can be multiplied by the number of springs. Assuming a spring of our dimensions has a spring rate of roughly $4\,\text{N}/\text{mm}$ [30], a force of $F = 16\,\text{N}$ should give a good estimate. The surface area that is pressed is defined as the copper seat with an inner radius of $6\,\text{mm}$ and an outer radius of $10.5\,\text{mm}$. This results in a pressure onto the copper seat of $P = \frac{F}{A_{cs}} = \frac{F}{\pi(r_o^2 - r_i^2)} = 0.069\,\frac{\text{N}}{\text{mm}^2}$ From the pressure we are now able to calculate the tightening index k which is defined as

$$k = \frac{P}{g \cdot R} = \frac{F}{g \cdot A \cdot R} \tag{24}$$

With the sealing surface A, the free-fall acceleration $g = 9.81\,\text{m}/\text{s}^2$ and the sealing factor R, which describes how a certain material will behave during the sealing. In [31] the sealing factor of soft copper at room temperature is given as $R_{cu} = 500\,\frac{\text{kg}}{\text{cm}^2} = 5 \times 10^6\,\frac{\text{kg}}{\text{m}^2}$. A change of R within the cryogenic setup is also expected, but it can be expected that this shift will go to higher R, since the modulus of elasticity of copper also rises when the temperature is lowered [32]. With these

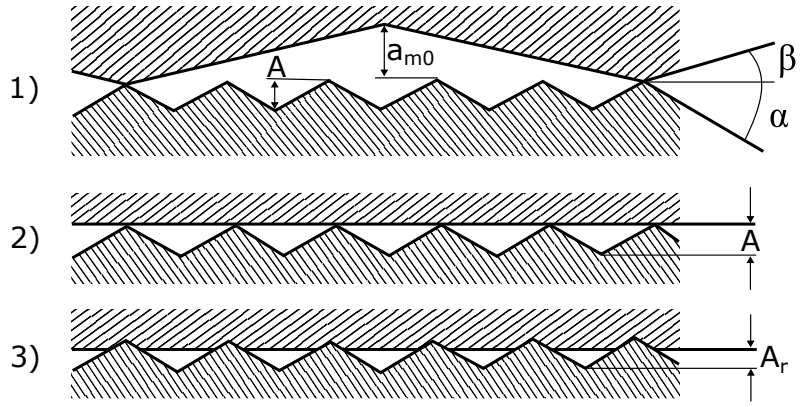

Figure 10: Waviness in the different stages of the sealing process. A and a_m0 are the waviness parameters of the corresponding surfaces. α and β represent the slopes of the triangles on these surfaces. (1) and (2) show the limits in which the accomodation stage takes place, where the gasket material flattens out onto the harder flange material. (3) shows the normal sealing stage where the gasket compresses into the flange material. Adapted from [29].

assumptions we finally get a tightening index of $k = 0.0014$. The accomodation stage usually ends at $k > 0.5$ to 0.6, so it can be assumed that the sealing of the valve will fully take place within this first stage.

For a round gasket in the accomodation stage [29] gives the conductance as

$$C_{\text{seal}} = C_0 \cdot F\left(\frac{a/2}{A}\right) \tag{25}$$

$$\text{with} \quad C_0 = 1.93 \cdot 10^4 \sqrt{\frac{T}{M}} \frac{2\pi}{8.12} \frac{A^2}{\ln(r_0/r_i)} \tag{26}$$

$$\text{and} \quad F\left(\frac{a/2}{A}\right) = \frac{2\left(1+2\frac{a/2}{A}\right)^2\left(1+\frac{a/2}{A}\right)\left(1+\frac{1}{\cos(\alpha)}\right)}{\left(1+\frac{1}{\cos(\alpha)}\right)\left(1+\frac{a/2}{A}\right)\left(1+2\frac{a/2}{A}\right)^{\frac{1}{2}}\left[\pi - \arctan\left(\frac{-1}{\left(1+2\frac{a/2}{A}\right)^{\frac{1}{2}}}\right)\right] + 1 + 2\frac{a/2}{A}} \tag{27}$$

To calculate this conductance we have to first give an estimate for the waviness parameters. We can again assume a waviness of $a = A = 10\,\mu\text{m}$ as a rather high surface roughness. In [31] they state that the peaks on most machined surfaces have slopes of 1° to 4°, so we will use $\alpha = 4^\circ$ for the investigation as a limit. Using these parameters/values results in a conductivity of $C_{\text{valve}} = 1.51 \times 10^{-4} \frac{\text{l}}{\text{s}}$ for the closed valve. This results in a reduction factor of $10\,000$. This also oversatisfies our requirement of a reduction factor of 100.

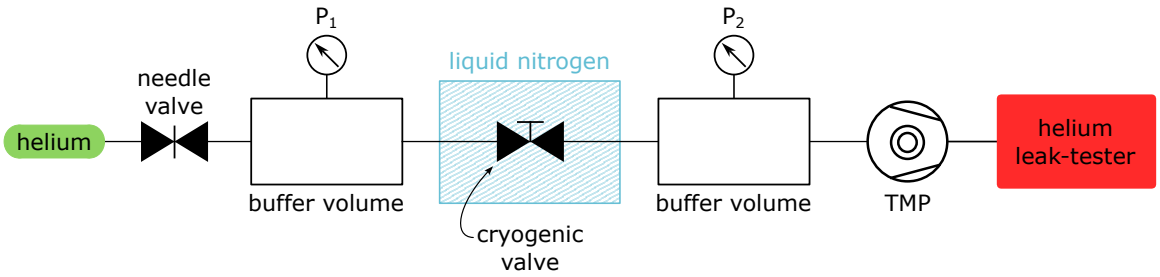

Figure 11: Measurement setup of the conductance testing. P_1 and P_2 represent the two PKR251 pressure gauges, while TMP stands for turbomolecular pump. The valve was submerged in liquid nitrogen during the 77 K runs as shown here.

6 Measurements

To see whether the new design ensures the required low inflow into the trap section in practice, two series of measurements were carried out.

6.1 Conductance measurement

6.1.1 Setup

The first conducted measurement was a conductance measurement of the cryovalve in its closed and open state. For this measurement a simple setup was used. The setup is shown in Figure 11. To get a good scale of how the valve performs, the idea is to directly measure its open and closed vacuum conductivity using Equation 9. This can be done by measuring the pressure drop over the valve for a given helium throughput. The throughput can be controlled and measured with a needle valve and a helium leak-tester. In this test a Pfeiffer ASM 340 was used to quantify the leak rate. Two full-range vacuum gauges, Pfeiffer PKR 251, were used to measure the helium pressure before and after the valve. Their pressure gradient in combination with the leakrate finally gives the conductance of the valve at a given time. Helium as a residual gas necessitates a correction of the measured pressures for the real helium pressures. A plot to fit the measurement data on to is found in the manual of the gauges [33]. Since we have two larger buffer volumes to fill, the pressure needs some time to settle at a equilibrium state. This does not take long, when the valve is fully opened, but will take several hours for measuring the closed conductance. This can be explained by the first buffer volume filling up until the remaining leak of the valve transmits the incoming leakrate through the needle valve into the leak-tester. This can then be compared to the conductance measured before the valve was closed at the same leakrate to give the ratio of how much the conductance could be lowered through the cryogenic valve.

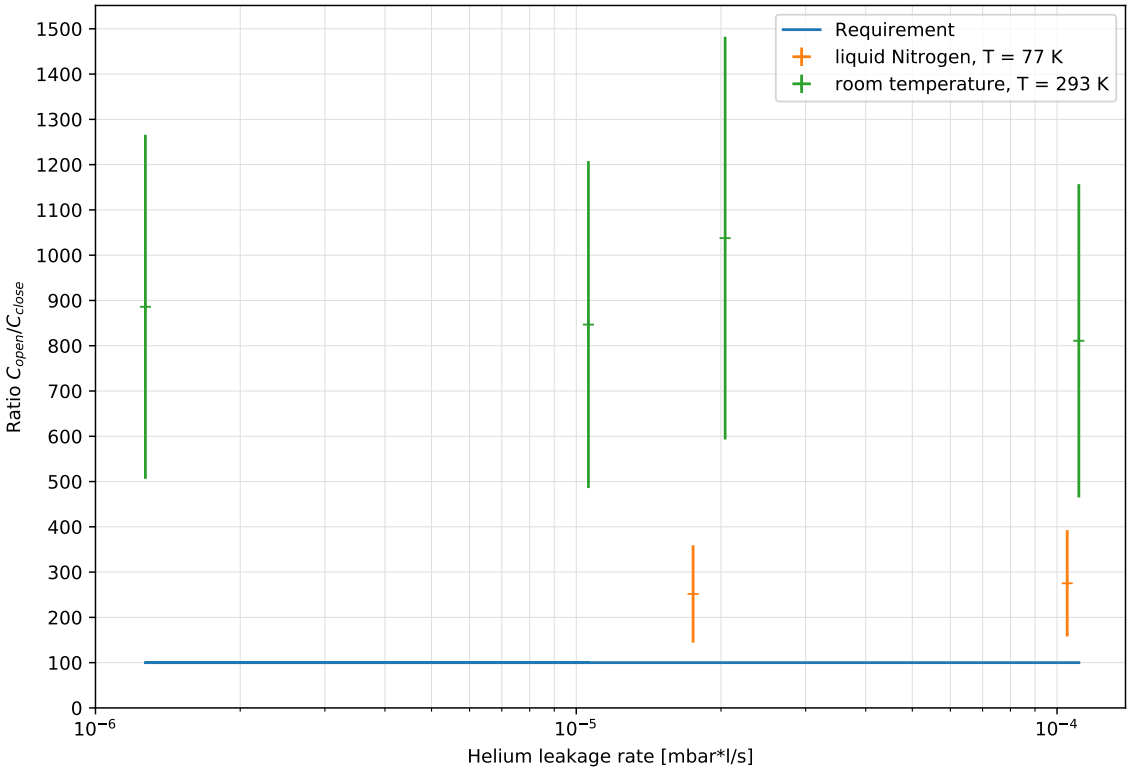

Figure 12: Results of the conductivity measurement.

6.1.2 Results

The results of the successful long-term measurements are shown in Figure 12. The measurements were all run at least 4 hours, while some were run over night. An error of 30 % is given for the pressure measurement of the vacuum gauges by Pfeiffer [33], while there was no error given by Pfeiffer for the leakage rate of the ASM 340. Looking at Equation 9 we can see that the ratio R given in the plot does not depend on the leakage rate anymore:

$$C_i = \frac{q}{\Delta p_i} \quad \Rightarrow \quad R = \frac{C_1}{C_2} = \frac{q}{\Delta p_1}\frac{\Delta p_2}{q} = \frac{\Delta p_2}{\Delta p_1} \tag{28}$$

When looking at the absolute conductivities, shifts can be identified between different measurements at the same leakrate, see Figure 13. These could indicate that the environmental factors like temperature, air humidity or pressure changed and that the calibration of the leak tester was off after several days or the needle valve was drifting. No further investigation of the systematics this leakage measurement introduces were made, since this was just measured to test the reproducability of the overall measurement over a wide range of helium leakage. Over the testing we saw that

the independent measurements got values that were a lot closer to each other than the errorbars would suggest. This could show that the pressure gauges have a such a high error, because of the grade of their calibration. Over the course of the measurements consistent results were obtained, the conductivity ratios measured were all consistent with one another showing that there was no statistical drift within the gauges. If the error on the pressure is due to calibration and assuming that the measured pressure is off by a factor of k at the measured pressure range, the error on the ratio should be a lot smaller since when dividing both pressures as in Equation 28 k would drop out. For this we also just have to look at the pressure gauge P_1 (see Figure 11) since the conductance is mainly given by the larger of the measured pressures. Additionally, it becomes apparent that at room temperature the reduction ratio within our testing between the open and the closed valve was around 1000, which is lower than what we calculated in the previous chapters. When we come back to the slot surface model, such a ratio is achieved for a slot height of $40\,\mu\mathrm{m}$. At liquid nitrogen temperature the ratio reduces to 270. In turn this translates to a slot height of $80\,\mu\mathrm{m}$ again in the slot model. This could be also be a hint for a deformation of the steel plate when being cooled down which could give a slot that is greater than the machined surface roughness would suggest.
From this testing, it can be expected that the requirements we put onto the valve hold up within the experiment. Further changes when cooled down to $4\,\mathrm{K}$ can be neglected since the mechanical properties do not change significantly below liquid nitrogen temperature [28]. It is also noted that the performance of the valve does not significantly deviate from the previous version [1]. Marco Orešković reported a reduction factor within his liquid nitrogen measurement campaign of 170 to 530, which is in line with the result found here.

6.2 Inspection of the closing of the valve

6.2.1 Setup

To see how the springs extend and how this effects the closing of the valve, the conductance was measured against the distance, as shown in the picture in the Appendix Figure 14. When the valve is closed this distance should be $3\,\mathrm{mm}$. For the plot this was in the end substracted from the remaining distance quantity to show how much way the valve still is able to close. This test should serve as a verification that the new alignment mechanism works without creating new issues during the closing process. Otherwise the same setup was used as in the previous measurement series.

6.2.2 Results

The results of this closing measurement are shown in Figure 13. The errorbars given here are again calculated from the $30\,\%$ error from the gauges. The two measurement runs were in principal set to the same leak rate, but a difference in the overall blockage was observed, at this point, the accuracy of the calibration is suspected to be the problem. This however is no problem, since from

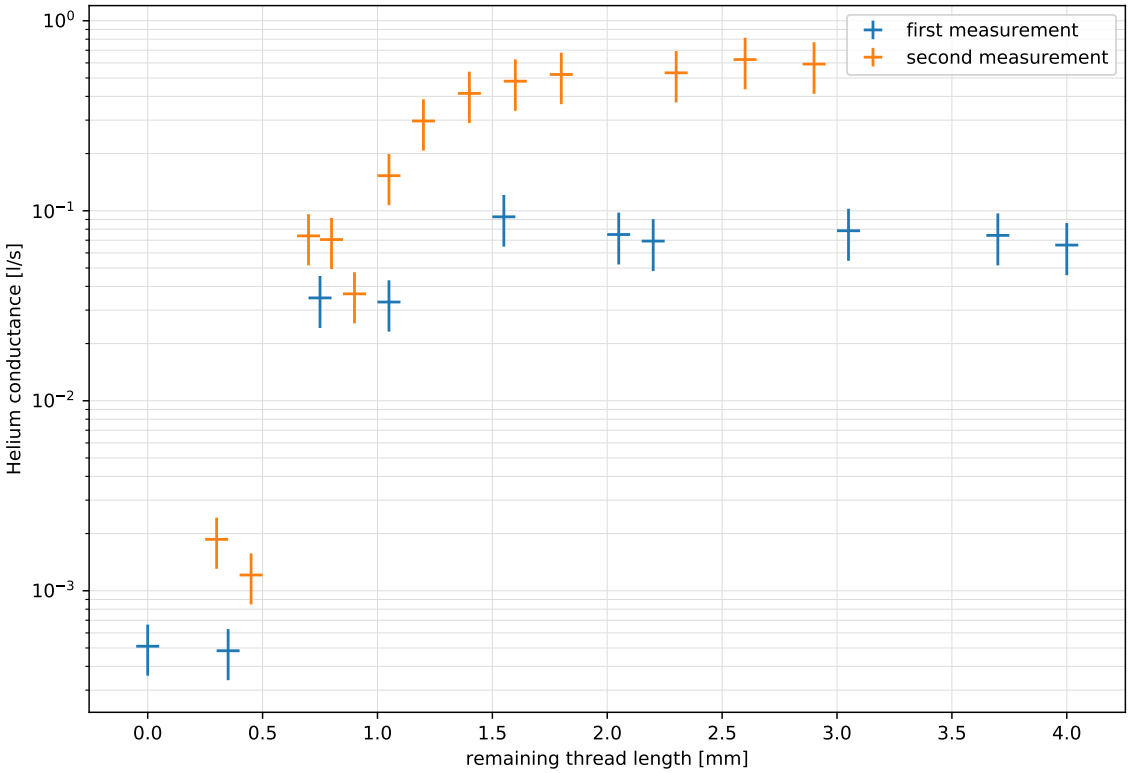

Figure 13: Measurement of the helium conductivity against the distance the valve has left to close, while being at a leakrate of roughly $1 \times 10^{-4}\,\mathrm{mbar} \cdot \mathrm{l/s}$

this we can still clearly see where the closing happens. At below $0.5\,\mathrm{mm}$ the valve behaves already identical to the closed state. Between $0.5\,\mathrm{mm}$ and $1.5\,\mathrm{mm}$ the closing appears to take place, while the conductance gradually get lower with the distance. Above $1.5\,\mathrm{mm}$ the valve is open. We also see that at $0\,\mathrm{mm}$ the sealing does not get worse again. The threaded M4 rod that moves the valves lid has a pitch of $0.7\,\mathrm{mm}$. The $0.5\,\mathrm{mm}$ for the closed valve then translate to a bit less then a turn of the threaded rod. With the gearbox which gives a translation of 1 to 4, this means that the last 3 turns at the room temperature section will be done while the valve is already closed. The tests were done at room temperature, so the exact distance will be slightly different in the cryogenic section.

7 Conclusion and Outlook

This thesis focused on the design of a cryogenic valve that is transparent for laser light over a wide frequency range. This new design is necessary for future measurement campaigns that involve laser spectroscopy or laser cooling. It allows to perform these measurements with the valve being closed. Since the vacuum in the trap chamber can be greatly improved by not opening the cryovalve towards the room temperature beamline. Within this thesis the previous valve was disassembled and a concept for a new design has been worked out. The new design was then manufactured in the workshop of the MPIK. Parts that were not changed compared to the previous version were reused. The new valve was tested in two measurement campaigns. First the ratio between the closed and the open conductances of the valve were measured with measurements taking up several hours. The conductance of the ion tube could be lowered by a factor of 270 at $77\,\mathrm{K}$ and at $293\,\mathrm{K}$ a factor of roughly 1000 was measured, exceeding the required minimum factor of 100. The requirement for this factor was set to 100 as a result of an investigation of the closing interface using a simple slot model as well as a sealing gasket model that also implements the surface roughness of the sealing surfaces. To analyze the situation with no valve installed, a calculation as well as a simulation were performed. These proved to be valuable tools to evaluate the pressure we would obtain without a valve. With room temperature residual gas particles, we found a pressure of $p = 2.8 \times 10^{-16}\,\mathrm{mbar}$ within the simulation and $p = 4.17 \times 10^{-15}\,\mathrm{mbar}$ for the calculation. These estimates rely on efficient cryo pumping, which in turn depends on the saturation of the ion tube with residual gas. The time for a monolayer to form along the complete $90\,\mathrm{cm}$ ion tube was found to be roughly at $4\,\mathrm{days}$ without the valve. With the valve this should be scaled by the previously stated factors, raising the saturation time to several years if the valve is not opened. For loading ions into the trap the valve still has to be opened. The time needed for loading should therefore be minimized to ensure the trap vacuum over a certain time period.

A second test was done to monitor how the valve closes. It was found that when the closing mechanism only has $0.5\,\mathrm{mm}$ of space left, the valve is already closed contributing to the spring mechanism that loads the two sealing surfaces with a force once they start to compress.

The new cryogenic valve that was installed at ALPHATRAP in the scope of this thesis will therefore provide new possibilities for interesting measurement campaigns. It enables the Penning trap experiment to use a wider range of measurement techniques without having to risk the trapped ions due to insufficient vacuum standing times.

From Section 3.4 we could argue that having some kind of flap inside the cryogenic section that can move in and out the ion tube could give a short term reduction of the influx into the traps by blocking of the room temperature solid angle that leads directly to the trap chamber. Such a system could be used in addition to the cryogenic valve, for example during ion loading when the ions are already in the trap, but the cryogenic valve could not be closed from the upper floor yet. Especially for ions with lower lifetimes this could prove beneficial.

8 Appendix

8.1 Measurement setup

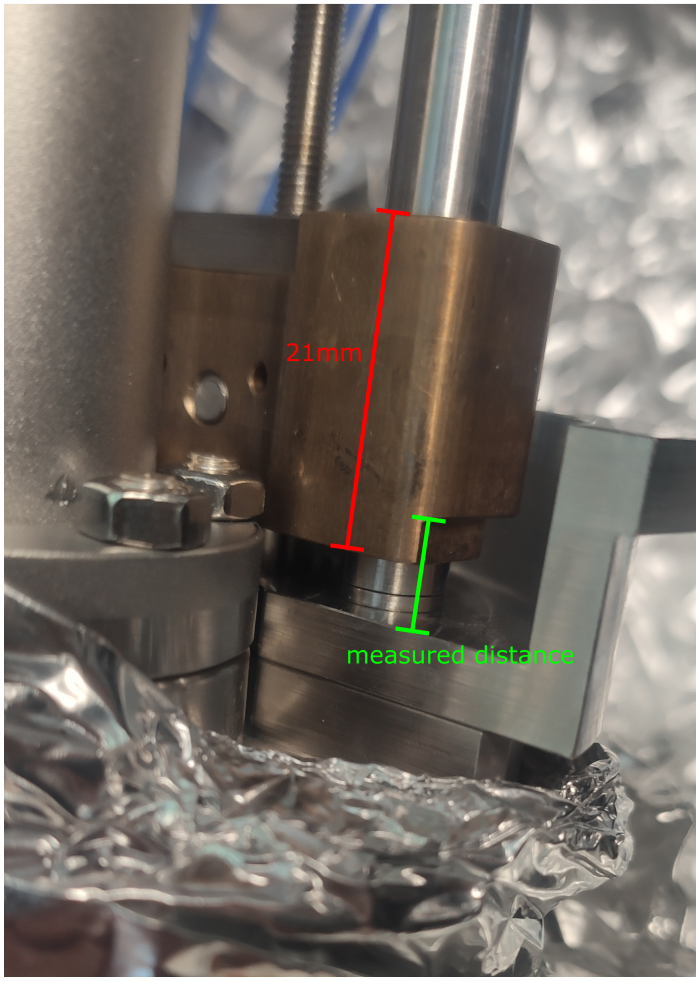

Figure 14: The distance was measured at the marker in the picture, between the little edge at the brass piece and the steel holder below. When fully closed this edge was designed to be 3 mm high.

References

[1] Marko Turkalj Orešković. *Development of a cryogenic vacuum valve and an electromechanical switch for ALPHATRAP*. Master thesis. 2014.

[2] Xing Fan et al. “Measurement of the electron magnetic moment”. In: *Physical review letters* **130**.7 (2023), p. 071801.

[3] Babak Abi et al. “Measurement of the positive muon anomalous magnetic moment to 0.46 ppm”. In: *Physical Review Letters* **126**.14 (2021), p. 141801.

[4] Alexandre Gumberidze et al. “Quantum electrodynamics in strong electric fields: the ground-state lamb shift in hydrogenlike uranium”. In: *Physical review letters* **94**.22 (2005), p. 223001.

[5] Anke Wagner et al. “g-factor of lithiumlike silicon $^{28}Si^{11+}$”. In: *Physical review letters* **110**.3 (2013), p. 033003.

[6] J Morgner et al. “Stringent test of QED with hydrogenlike tin”. In: *arXiv preprint arXiv:2307.06613* (2023).

[7] MG Kozlov et al. “Highly charged ions: Optical clocks and applications in fundamental physics”. In: *Reviews of Modern Physics* **90**.4 (2018), p. 045005.

[8] Sven Sturm et al. “The ALPHATRAP experiment”. In: *The European Physical Journal Special Topics* **227** (2019), pp. 1425–1491.

[9] AJ González Martınez et al. “The Heidelberg EBIT: Present results and future perspectives”. In: *Journal of Physics: Conference Series*. Vol. **72**. 1. IOP Publishing. 2007, p. 012001.

[10] Peter Micke et al. “The Heidelberg compact electron beam ion traps”. In: *Review of Scientific Instruments* **89**.6 (2018).

[11] Tim Sailer. *A Laser Ion Source for the ALPHATRAP Experiment*. Master thesis. 2017.

[12] Simon Heidrich. *Recommissionig of the Hyper-EBIT by measuring x-ray spectra of highly charged ions*. Bachelor thesis. 2022.

[13] Sangeetha Sasidharan et al. “LIONTRAP Experiment: the Proton Mass, the Deuteron Mass and More”. In: *FFK 2021* (2021), p. 51.

[14] A Mooser et al. “Direct high-precision measurement of the magnetic moment of the proton”. In: *Nature* **509**.7502 (2014), pp. 596–599.

[15] Christian Smorra and Andreas Mooser. “Precision measurements of the fundamental properties of the proton and antiproton”. In: *Journal of Physics: Conference Series*. Vol. 1412. 3. IOP Publishing. 2020, p. 032001.

[16] Alexander Egl et al. “Application of the continuous Stern-Gerlach effect for laser spectroscopy of the Ar 13+ 40 fine structure in a Penning trap”. In: *Physical Review Letters* **123**.12 (2019), p. 123001.

[17] Alexander Egl. “High-precision Laser Spectroscopy of the Fine Structure in $^{40}Ar^{13+}$ at ALPHATRAP”. PhD thesis. Ruprecht-Karls-Universität Heidelberg, 2020.

[18] Karl Jousten. *Handbuch Vakuumtechnik*. Springer-Verlag, 2018.

[19] International Organization for Standardization. *ISO 3529-1:2019: Vacuum technology — Vocabulary — Part 1: General terms*. 2019.

[20] Torsten Fließbach. *Statistische Physik: Lehrbuch zur Theoretischen Physik IV*. Springer-Verlag, 2018.

[21] Ahmad Fauzi Ismail, K Chandra Khulbe, and Takeshi Matsuura. “Gas separation membranes”. In: *Switz. Springer* **10** (2015), pp. 973–978.

[22] RE Olson and A Salop. “Electron transfer between multicharged ions and neutral species”. In: *Physical Review A* **14**.2 (1976), p. 579.

[23] Nikolaus Helmut Hermanspahn. “Das magnetische Moment des gebundenen Elektrons in wasserstoffartigem Kohlenstoff (C^{5+})”. PhD thesis. Ges. für Schwerionenforschung, 2000.

[24] National Institute fo Standards and Technology - NIST. *Atomic Spectra Database Ionization Energies*. `https://physics.nist.gov/PhysRefData/ASD/ionEnergy.html`. last accessed on 4th of September 2023.

[25] Florian Köhler et al. “The electron mass from g-factor measurements on hydrogen-like carbon $^{12}C^{5+}$”. In: *Journal of Physics B: Atomic, Molecular and Optical Physics* **48**.14 (2015), p. 144032.

[26] Werner G Baechler. “Cryopumps for research and industry”. In: *Vacuum* **37**.1-2 (1987), pp. 21–29.

[27] *Private communication with Sven Sturm*.

[28] National Institute fo Standards and Technology - NIST. *Material Properties: 304 Stainless (UNS S30400)*. `https://trc.nist.gov/cryogenics/materials/304Stainless/304Stainless_rev.htm`. last accessed on 21st of September 2023.

[29] Alexander Roth and Abraham Inbar. “The force cycle of vacuum gasket seals”. In: *Vacuum* **17**.1 (1967), pp. 5–13.

[30] Gutekunst + Co.KG. *Compression spring calculation*. `https://www.federnshop.com/en/calculation/compression_springs.html`. last accessed on 22nd of September 2023.

[31] Alexander Roth. *Vacuum technology.* Tech. rep. ISRAEL ATOMIC ENERGY COMMISSION, YAVNE. SOREQ NUCLEAR RESEARCH CENTER., 1972.

[32] HM Ledbetter. “Temperature behaviour of Young’s moduli of forty engineering alloys”. In: *Cryogenics* **22**.12 (1982), pp. 653–656.

[33] Pfeiffer Vacuum GmbH. *BETRIEBSANLEITUNG - PKR 251 - Compact FullRange® Gauge, FPM gedichtet*. https://www-acc.gsi.de/wiki/pub/IC/MTF_Docu/Pfeiffer_BG5155BDE_C.pdf. last accessed on 16th of September 2023.

Acknowledgements

First of all, I would like to thank Sven Sturm for the supervision of my work, his time and patience during all phases of this work!

Many thanks to the ALPHATRAP team for their continued support, especially Jonathan and Charlotte for assistance with measurements and proofreading.

Furthermore, I want to thank all the nice people from the other Penning trap experiments at MPIK, who made working here very enjoyable.

Finally, I would like to thank Tabita for always being there for me when I needed her!

Erklärung

Ich versichere, dass ich diese Arbeit selbstständig verfasst und keine anderen als die angegebenen Quellen und Hilfsmittel benutzt habe.

Heidelberg, den 23.09.2023,